Marangoni Interaction of a Liquid Droplet Falling onto a Liquid Pool

The study of flow behavior in a simulated GMAW weld pool offers insight into inclusion distribution in welds

BY R. T. C. CHOO, K. MUKAI AND J. M. TOGURI

ABSTRACT. A water-alcohol physical model was built to study the relative strengths of the driving forces responsible for fluid motion when a liquid droplet falls onto an isothermal liquid bath. This model simulates the gas metal arc welding (GMAW) operation in which a filler metal is used. The droplet has a surface tension and density that are different from the pool. It was found that the surface tension force generated the strongest flow when compared with buoyancy force and stirring force induced by the falling droplet. Furthermore, the relative difference in the surface tension between the drop and the liquid pool determines the flow pattern direction. If the droplet has a larger surface tension than the pool, then the surface flow is directed inward and a deep flow loop is created. The reverse occurs when the droplet has a lower surface tension in which an outward surface flow is generated. These observations suggest that the role of the droplet-induced Marangoni flow should not be precluded from flow analyses in GMAW. Furthermore, these flow behaviors are suspected to be responsible for inclusion distribution in the weldment.

Introduction

In gas tungsten arc welding (GTAW), the importance of surface tension driven or Marangoni flow has been widely investigated (Refs. 1–6). This thermocapillary driven convection is known to affect the structure and properties of the final weldment through the shape of the weld pool and its associated solidification phenomena (Refs. 1–8). The bulk of the analyses on Marangoni flow tend to focus on the role of surface active species, primarily S, although O, Se and Te are also known to affect flow behavior for iron-based alloys (Ref. 2). This approach is deemed justifiable in the case of autogenous welding since Marangoni flow has been identified as the most dominant factor controlling weld pool convection.

When filler metal is used, such as in gas metal arc welding (GMAW), there has been extensive characterization on the filler metal behavior in the welding arc (Refs. 9–15). Much has been studied on the droplet behavior in flight, droplet detachment rates, droplet transfer mechanism and droplet stability. However, the Marangoni interaction of the molten filler metal when it touches the weld pool has not been addressed. Since convective flow in the weld pool is largely controlled by surface tension effect at low arc currents, this interaction should affect the outcome of the flow behavior in the weld pool and thus deserves further study.

In this paper, a water-alcohol physical model has been designed to simulate the interaction between a liquid droplet (filler metal) and a liquid bath (weld pool) at ambient conditions. This low-temperature model permits direct observation and characterization of the flow behavior. Furthermore, the model offers a means of studying and visualizing particle (inclusion) behavior under various flow conditions. It is felt that these scoping studies will permit more detailed experimental and computational work to be initiated.

R. T. C. CHOO and J. M. TOGURI are with the Department of Metallurgy and Materials Science, University of Toronto, Toronto, Canada. K. MUKAI is with the Department of Materials Science and Engineering, Kyushu Institute of Technology, Kitakyushu, Japan.

KEY WORDS

Physical Modeling
Marangoni Interaction
Liquid Droplet Model
Filler Metal Droplet
Weld Pool Model
GMAW Model
Water-Alcohol Model
Driving Forces
Fluid Motion
Surface Tension

Description of Marangoni Behavior in the Weld Pool

Marangoni flow is defined as the flow attributed to surface tension gradients. In welding, this thermocapillary action is given as (Refs. 3–6):

$$\tau_{M(T)} = -\mu \frac{\partial \gamma}{\partial z} = \left(\frac{\partial \gamma}{\partial T}\right)\left(\frac{\partial T}{\partial x}\right) \quad (1)$$

where the Marangoni shear, $\tau_{M(T)}$, is due to the surface tension dependence on temperature. μ is the viscosity of the weld pool, u is the radial surface velocity, z is the axial coordinate, γ is the surface tension, T is the surface temperature, and x is the radial surface coordinate.

The mechanism responsible for this surface motion can be described in the following terms: 1) as the temperature increases, the surface tension of pure liquid generally decreases; 2) this will cause the surface tension coefficient, $\partial\gamma/\partial T$, to be less than zero; 3) the weld pool surface temperature profile is such that it is hotter in the middle of the pool than at the edges; 4) thus, if $\partial\gamma/\partial T < 0$, then the surface tensions are lowest at the center of the pool and highest at the edges; 5) as a result, an outward surface flow field is generated; 6) sometimes, the presence of surface active species such as S can produce positive $\partial\gamma/\partial T$ due to segregation effects (Ref. 2). In this instance, an inward surface flow loop results.

By the same token that Marangoni shear can be temperature driven, it can also be concentration driven:

$$\tau_{M(C)} = -\mu \frac{\partial u}{\partial z} = \left(\frac{\partial \gamma}{\partial C}\right)\left(\frac{\partial C}{\partial x}\right) \quad (2)$$

where $\tau_{M(C)}$ is the Marangoni shear attributed to the surface tension dependence on concentration and C is the sur-

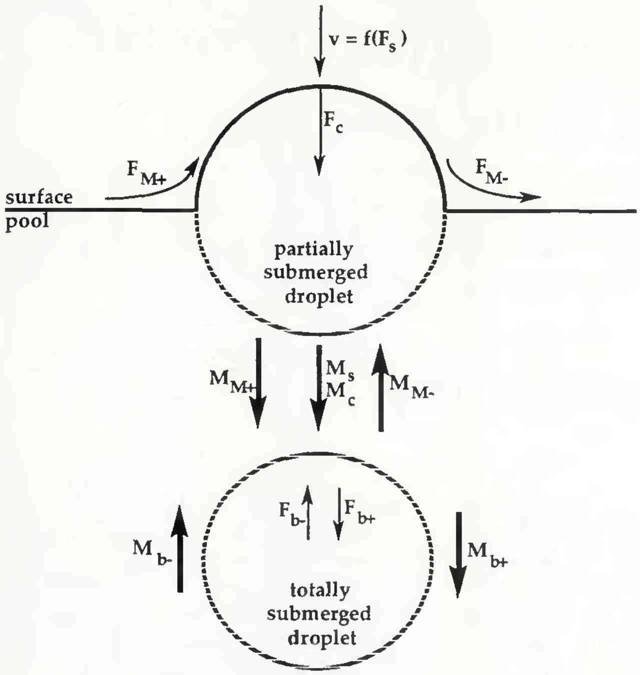

Fig. 1 — Forces and motions induced when a droplet falls onto a liquid pool. The top droplet is partially submerged while the lower droplet is totally submerged. The light arrows indicate the forces acting while the bold arrows show the motion induced by the corresponding forces. F = direction of force. M = direction of motion. Subscripts: c = curvature, s = stirring, b+ = buoyancy ($\rho_d > \rho_p$), b- = buoyancy ($\rho_d < \rho_p$), M+ = Marangoni ($\gamma_d > \gamma_p$), and M- = Marangoni ($\gamma_d < \gamma_p$).

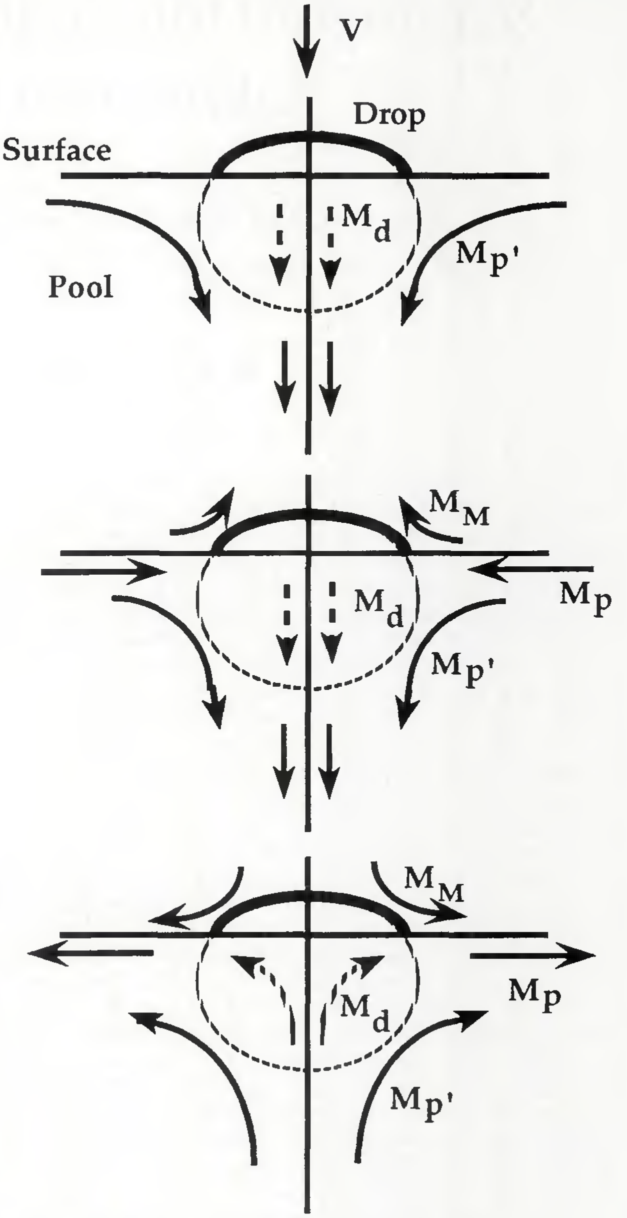

Fig. 2 — Droplet flow behavior when just in contact with the liquid pool. Top — $\gamma_d = \gamma_p$: droplet enters pool with velocity, v, and penetrates into pool. Center — $\gamma_d > \gamma_p$: Marangoni forces (M_M) cause pool's surface to be drawn toward droplet (M_p). The droplet is "injected" into the pool as a result (M_d). Lower — $\gamma_d < \gamma_p$: Marangoni forces (M_M) cause droplet's surface to be drawn away from droplet (M_p). The droplet is "spread" out as a result (M_d). M_M = direction of Marangoni motion induced by Marangoni forces; M_p = direction of pool surface motion; $M_{p'}$ = direction of pool bulk motion; M_d = direction of droplet motion.

face concentration of the molten pool. An example of such a situation occurring is when the welding process is nonautogenous, whereby a filler metal is added. To some extent, the concentration is temperature dependent but this $\partial C/\partial x$ ($\partial C/\partial T \bullet \partial T/\partial x$) is not considered to be significant, as the pool is rigorously stirred during the welding operation. This assumption is routinely employed in modeling GTAW processes.

The flow mechanism is no different from the temperature-driven case described above except that it is now concentration driven. From Equation 2, it can be seen that the interaction is twofold: the γ dependence on concentration, as well as the spatial dependence of the concentration on the weld pool surface. The surface tension is known to exhibit strong dependence with composition (Ref. 16).

It can be deduced that $\partial\gamma/\partial x$ (Equation 2) is very large when the filler metal first comes into contact with the weld pool surface. Actually, it is the sign of $\partial\gamma/\partial x$, which determines the direction of flow. The practical implication is whether the droplet will penetrate into the weld pool or spread out onto the surface. As a result, one may also suspect that the inclusion distribution is affected by this flow circulation.

The key point, then, is to determine which is the larger of the two driving shears, $\tau_{M(T)}$ or $\tau_{M(C)}$, as well as when these shears are active. It is clear that $\tau_{M(T)}$ is dominant during the welding operation when no drop touches the pool, while $\tau_{M(C)}$ is dominant when the drop touches the pool. Furthermore, $\tau_{M(C)}$ tends to be a local phenomenon in the vicinity of the drop. This dual action of Marangoni forces can result in a complex flow behavior. In order to reduce the complexity of the problem and to examine the nature of the concentration-Marangoni effect, only the concentration-capillary action will be examined in this paper. This parametric analysis will allow for the elucidation of the various Marangoni mechanisms in the welding operation.

Falling Liquid Droplet onto a Liquid Pool

When a liquid droplet falls onto an isothermal liquid pool, three types of flow motion can be generated as a re-

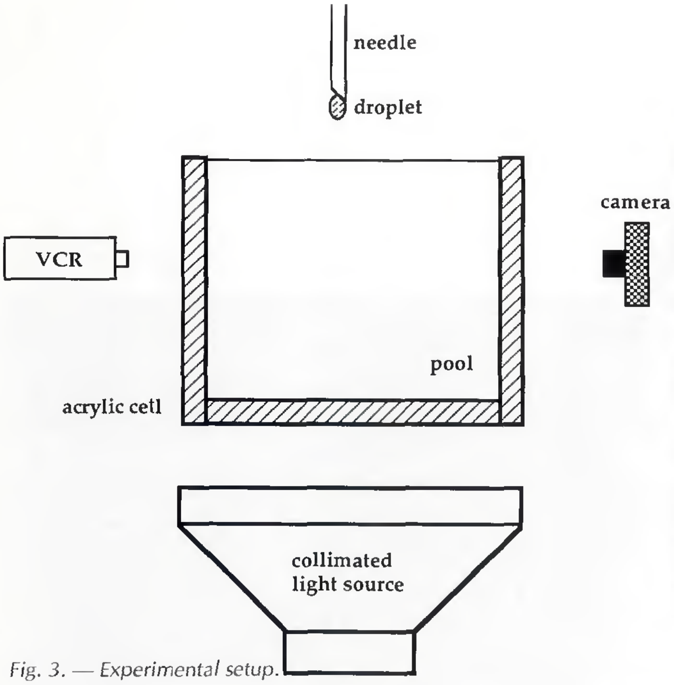

Fig. 3. — Experimental setup.

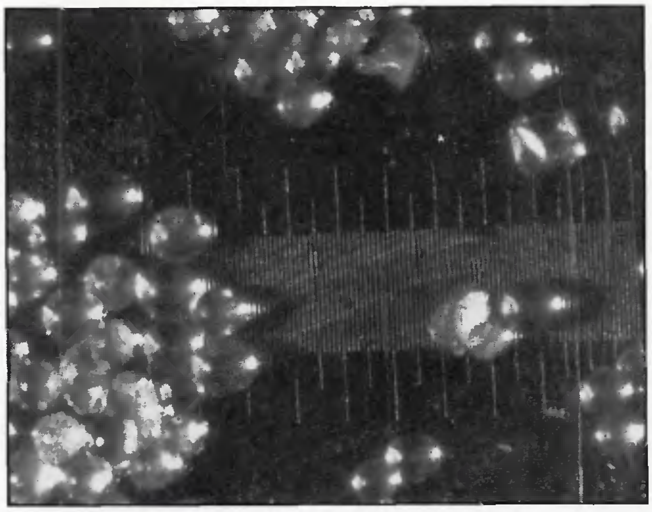

Fig. 4. — Photomicrograph of hollow glass beads (100 μm diameter). Each minor division on the scale is 0.01 mm, while the major division is 0.1 mm.

sult of the surface tension difference between the droplet and the pool:

Case A: $\Delta\gamma = \gamma_d - \gamma_p = 0$.
Case B: $\Delta\gamma = \gamma_d - \gamma_p > 0$.
Case C: $\Delta\gamma = \gamma_d - \gamma_p < 0$.

The subscript d and p are for droplet and pool, respectively.

There are four forces that are responsible for driving fluid flow motion in the pool as a result of the falling droplet — Fig. 1:

1) "Stirring" force, F_s, due to the momentum of the free falling droplet onto the pool. The stirring force is a function of the droplet velocity as the droplet enters the pool and it induces a downward motion, M_s.

2) The "curvature" force, F_c, due to the curvature of the droplet as given by the Young and Laplace equation $P_d - P_p = 2\gamma/r$ where P_d and P_p are the pressures of the droplet and pool, respectively, and r is the radius of the droplet. This force acts when the drop is partially submerged and it also induces a downward motion, M_c.

3) Buoyancy force (F_{b+} or F_{b-}) due to the density difference between the droplet and pool ($\Delta\rho = \rho_d - \rho_d$). The buoyancy force is active when the droplet (assuming the droplet maintains some integrity) is submerged and is a function of $\Delta\rho$; thus, it can induce either an upward (M_{b-}) or a downward (M_{b+}) motion.

4) Marangoni force (F_{M+} or F_{M-}) due to the surface tension difference between the droplet and pool. This Marangoni force acts when the droplet is partially submerged and can be in either direction depending on the sign of $\Delta\gamma$. The induced motions (M_{M+} or M_{M-}) are shown likewise.

Having described the driving forces for the droplet-pool interaction, we shall now discuss how these forces manifest themselves with respect to the three cases outlined above, which are also the cases to be examined experimentally.

Case A

This scenario is the base test; the simplest example being a water drop falling onto a water pool — Fig. 2, top. The two forces that are active both produce similar downward motions (M_d). The stirring force, on the one hand, is a result of the kinetic energy of the drop entering the pool. Naturally, this stirring force is a function of the height at which the drop falls. The curvature force, on the other hand, is a function of the curvature of the drop that is above the free surface datum — Fig. 1. As the drop penetrates into the pool, its shear action will also drag adjacent layers of liquid ($M_{p'}$). A distinct flow pattern is not expected to be generated in this type of flow motion.

Case B

In order to simplify the analysis, let us assume that the droplet falls from a short distance from the free surface such that the falling momentum is not large enough for the droplet to penetrate into the pool. On touching the surface, as $\gamma_d > \gamma_p$ (Fig. 2, center), the drop will have higher surface tension. This will cause it to pull the adjacent surface toward itself (M_M). This sudden "pull" is transmitted along the surface of the pool. As a result, an inward surface flow (M_p) toward the droplet is created. This inward surface flow will also cause the droplet to be "injected" into the bulk liquid (M_d). A distinctive flow loop ($M_{p'}$) may be generated as a result of the flow action M_p.

Case C

This is the reverse of Case B, and by similar arguments as above, an outward surface flow (M_p in Fig. 2, lower) is produced. The flow is generated because the pool's surface adjacent to the drop's surface has a higher surface tension and thus pulls the drop's surface away from the center of the drop (M_M) onto the surface of the pool. As the drop spreads out (M_d), its shear action will also drag adjacent bulk liquid molecules ($M_{p'}$). A distinctive flow pattern may also be generated as the Marangoni forces continue to act as the droplet is diluted.

The key point here is to identify critical parameters that control the quality of the weldment as governed by convective flows. In view of the concepts presented above, the water-alcohol model employed in this study serves to illustrate the nature and relative strengths of the driving forces attributed to the drop (filler metal). In order to obtain more detailed information of the actual welding system, a mathematical model is required that solves for both the temperature and concentration dependence of surface tension. This model is currently under development. Nevertheless, valuable insights can still be gained from the qualitative observations, which should provide a deeper understanding to more elaborate analyses.

Fig. 5. — Behavior of falling drop on a liquid pool. Case numbers correspond to Table 1. The left-hand photograph of each pair shows the drop motion at ⅛ s after the drop is discharged from the needle onto the liquid surface, while the right-hand photograph shows the results at 1 s.

Case 1

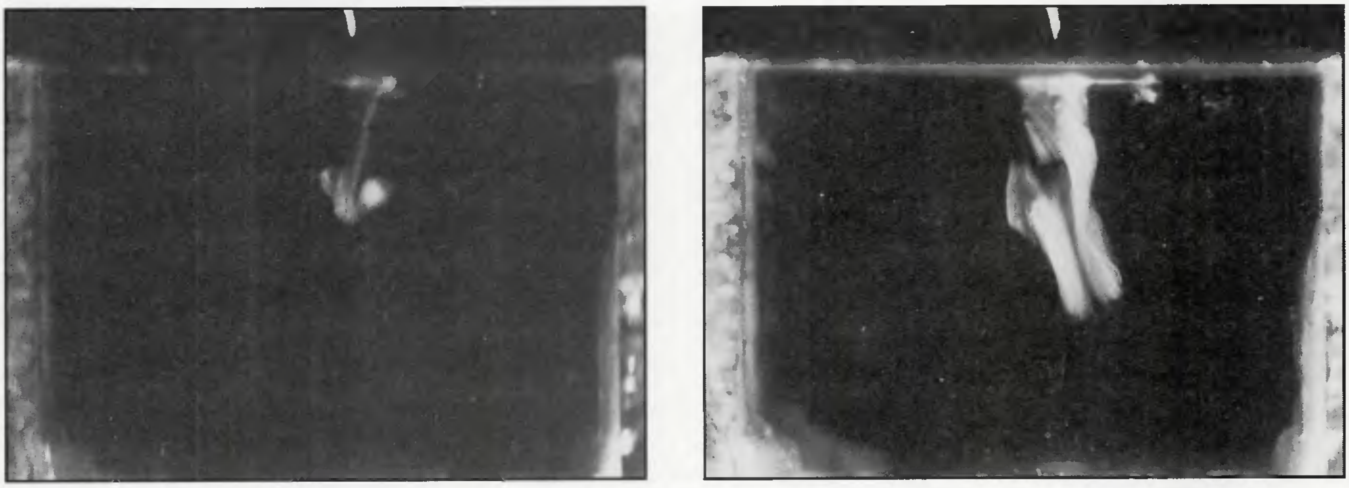

Case 2

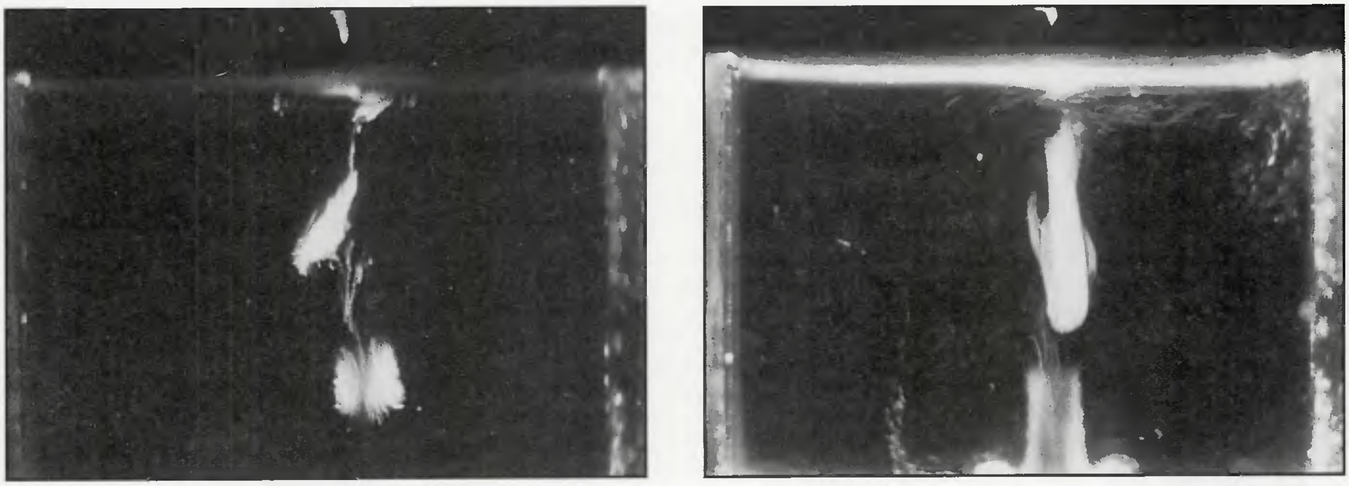

Case 3

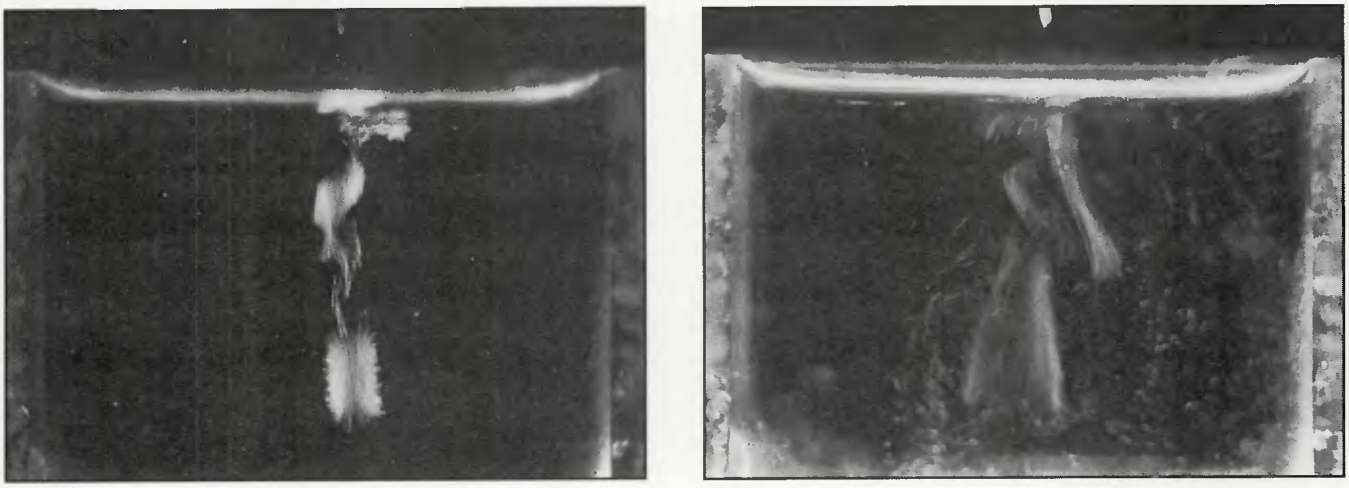

Case 4

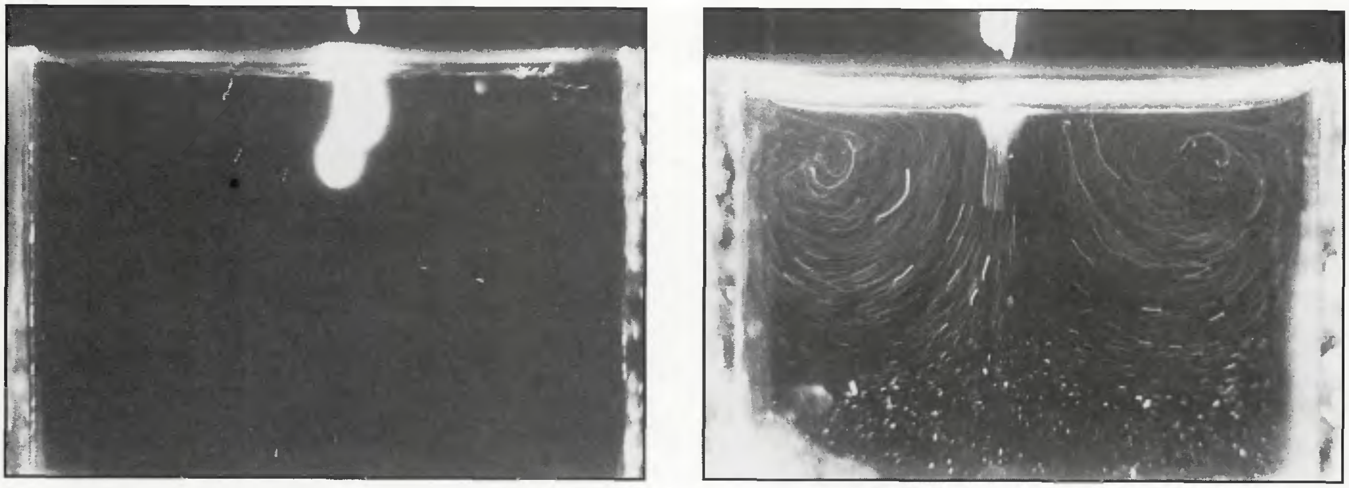

Case 5

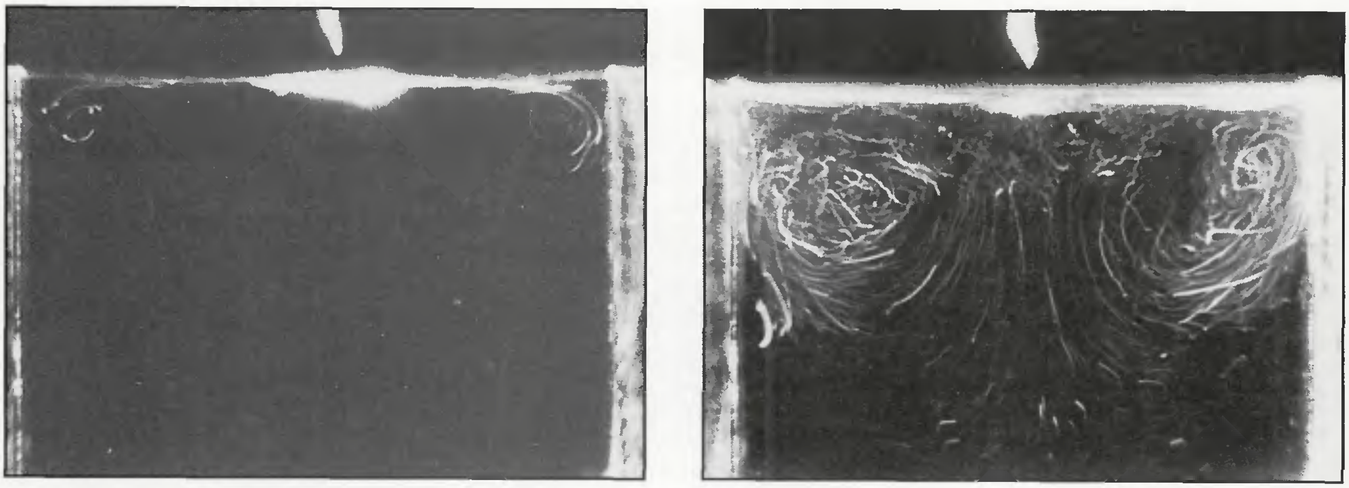

Case 6

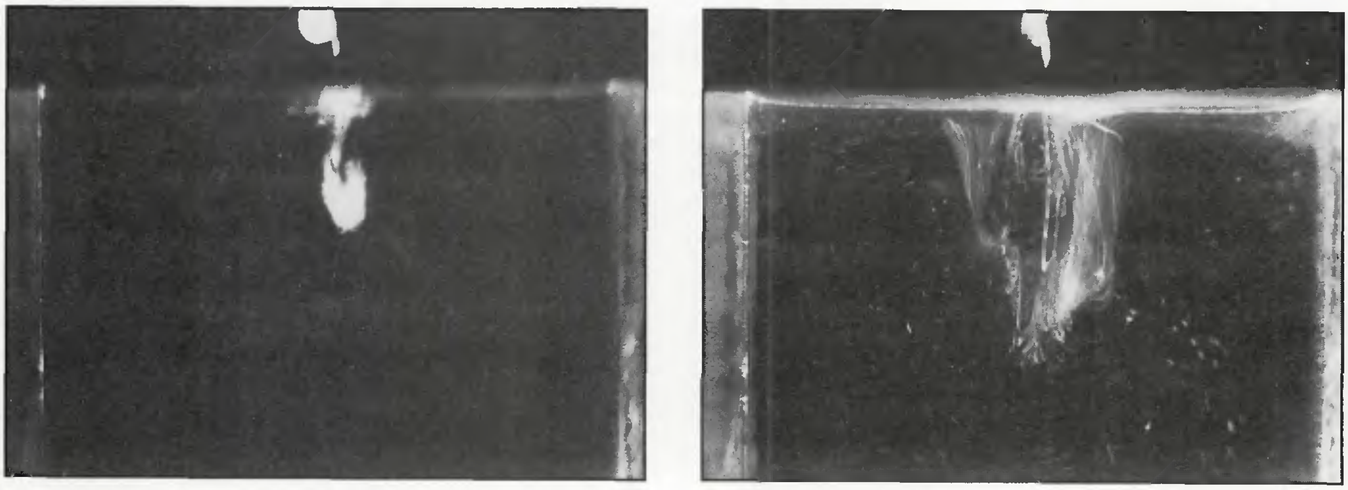

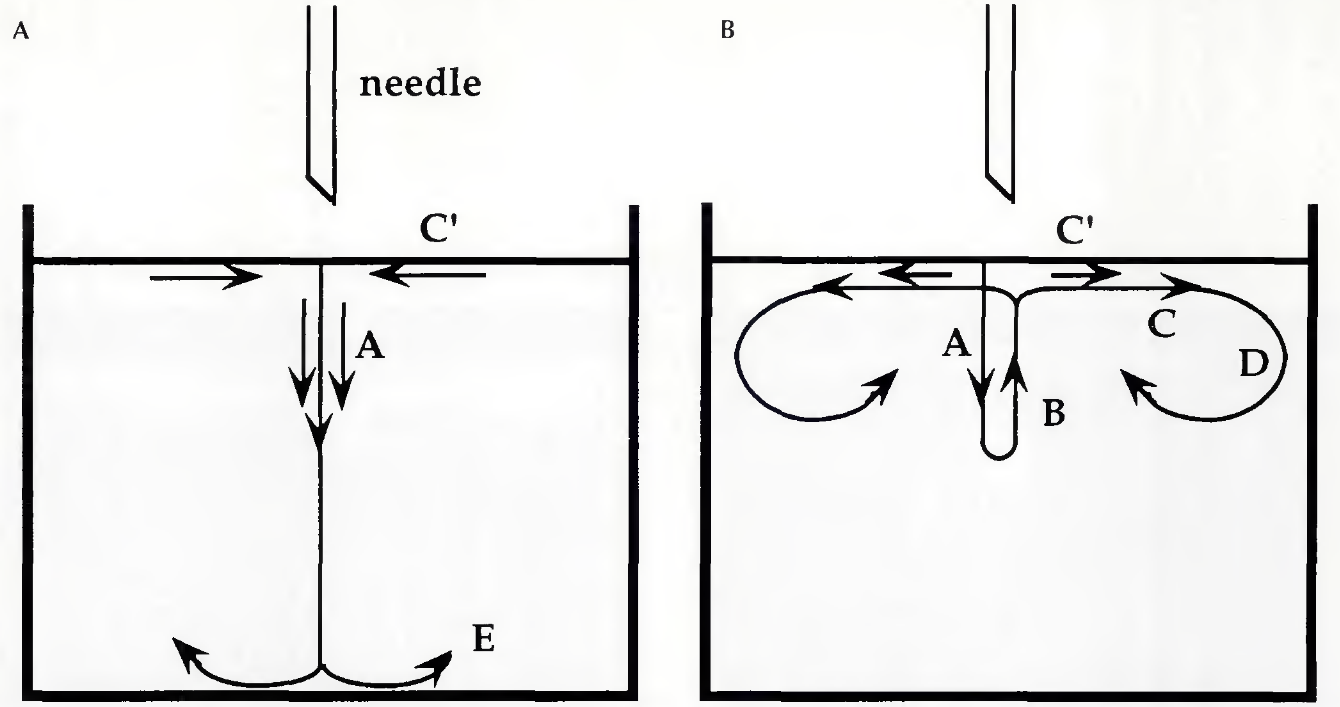

Fig. 6. — Schematic representation of drop behavior in experimental cell. A — Type 1 flow: $\gamma_d > \gamma_p$; B — Type II flow: $\gamma_d < \gamma_p$. A = Penetrating flow due to falling drop and/or Marangoni flow. B = Rising flow due to buoyancy. C = Spreading flow due to later stages of Marangoni effect. C' = Spreading or enclosing flow due to initial stages of Marangoni effect. D = Toroidal flow at far wall. E = Swirling flow at bottom wall due to droplet collision with wall.

Experimental

The flow behavior in the pool was observed by means of the particle tracking technique using a dark-field illumination method (Ref. 17). An acrylic cell (Fig. 3) 40 mm (1.6 in.) long, 20 mm (0.78 in.) wide, and 30 (1.2 in.) mm high served as the pool container. A collimated light source was located below the cell, which radiated a narrow beam of light (2 mm wide and spanning 40 mm) through the cell. Only the vertical central section was illuminated. The collimated light was projected onto the base of the cell, which has the dimensions of 40 mm long and 20 mm wide. The purpose of using the collimated light was to maintain a constant beam width.

Liquid droplets were created by means of a syringe-needle (1.25-mm, 0.05-in. OD) arrangement located 3 mm (0.12 in.) from the surface. The droplets are ellipsoidal in shape with 3.0 mm and 2.6 mm (0.1 in.) in the major and minor axes, respectively, for water and 2.5 (0.1 in.) mm and 2.2 mm (0.09 in.) in the major and minor axes, respectively, for 34% alcohol. The particles (Fig. 4) employed for flow tracking were hollow glass spheres (mean size 100 µm diameter and mean density 0.3 g/cm^3). The liquids used were distilled water, ethyl alcohol (C_2H_5OH) and sodium chloride (NaCl). These liquids were chosen so as to show the effects of surface tension driven flow via $\gamma_d - \gamma_p > 0$, $\gamma_d - \gamma_p = 0$, $\gamma_d - \gamma_p < 0$ as given in Table 1.

The observed fluid motion in the pool due to the liquid drop falling onto the pool was recorded by time-lapse photography and videotapes. A relay was used to synchronize the camera shots and the instant the drop was discharged. Table 1 (Refs. 18–20) shows the experimental conditions employed and the cases studied. All experiments, except for Case 6, were performed at 298 K.

Table 1—Composition of Droplets and Bulk Liquids and Their Physical Properties[a]

Case	Droplet	Pool	$\gamma_d - \gamma_p$ (dyne/cm)	$\rho_d - \rho_p$ (g/cm^3)	μ_p (mP)
1	water	water	0	0	8.9
2	3% alcohol	8% alcohol	9.9	0.0081	12.4
3	water	8% alcohol	22.3	0.0137	12.4
4	8% alcohol	3% alcohol	−9.9	−0.0081	10.2
5	34% alcohol	water	−41.0	−0.05387	8.9
6	water	7.6% NaCl	−2.5 (293 K)	−0.0538	10.1

(a) Composition is in mass-%. Ethyl alcohol (C_2H_5OH) is used. The viscosities of the bulk liquids are given at the melting point. The pool viscosities are of the same order of magnitude for the cases examined and thus not expected to affect the flow rates significantly.

Experimental Results

Figure 5A and B shows the time-lapsed photographs of the experimental conditions given in Table 1. The left side (Fig. 5A) is for a ⅛-s exposure, while the right side (Fig. 5B) is for a 1.0-s exposure. The schematic representation of the fluid flow in Fig. 5A and B are summarized in Fig. 6A and B to permit ease of discussion of results. Figure 6A and B is drawn along the concepts developed in Fig. 2A, B and C. The selection of results presented is meant to illustrate which of the three driving forces described above is most critical in controlling fluid motion.

Case 1

Case 1 (Fig. 5) is the null test showing the depth of penetration due to the water droplet impinging onto the pool. In this instance, both the buoyancy and Marangoni forces are zero. At ⅛ s, the drop appears to penetrate up to one-third the depth of the pool (~10 mm, 0.4 in.). Note that 1 s after impact, there is no definitive flow pattern being developed in the pool. In fact, the flow at 1 s is quite similar to that at ⅛ s. The type of flow generated can be said to be of Type 1 shown in Fig. 6A without the C′ and E flows.

Cases 2 and 3

In Case 2 (Fig. 5), the droplet penetrated deep into the bath and struck the bottom of the cell within 1 s. Furthermore, a secondary flow loop (E in Fig. 6A) is also generated when the "drop" hits the bottom. Some enclosing surface flow (C′) is also evident due to Marangoni effect. Case 3 is similar to Case 2 except that the Dg is 2.25 times larger while Dr is about 1.69 times larger. It is noted that the flow loops in Case 3 are much more intense, indicating that stronger driving forces are active. The flow patterns in Cases 2 and 3 are shown schematically in Fig. 6A as Type 1 flow.

In Cases 2 and 3, all four forces (stirring, curvature, buoyancy, and Marangoni) are present. At ⅛ s, note that Cases 2 and 3 penetrated deeper into the pool than the null test (Case 1). The forces that cause this deeper penetration are due to buoyancy and Marangoni effects. The buoyancy forces cause the droplet to sink as it is denser than the bulk liquid, while the Marangoni force causes the droplet to penetrate by means of the mechanism shown in Fig. 2B. The stirring force, F_s, is not responsible for the deeper penetration since it can be assumed that the droplet is of the same size and thus of the same velocity, v, as it enters the pool. As for the curvature force, F_c in Case 3 should be identical to that in Case 1 as the droplets are both water. In Case 2, as γ3%-alc < γH_2O, a weaker surface curvature force for the alcohol droplet results in comparison with the water droplet. This means that F_c (Case 1) = F_c (Case 3) > F_c (Case 2), and so the curvature force is also not responsible for the deeper penetration in Cases 2 and 3.

In order to determine the relative strength of the buoyancy force, the same volume of fluid was introduced slowly into the acrylic cell below the surface of the pool. Here, the stirring, curvature, and Marangoni forces were absent. It was observed that the downward flow velocities due to buoyancy were about 30 times smaller than those observed in Case 3. Thus, it was ascertained that the deeper penetrating flows (A) in Cases 2 and 3 were due primarily to Marangoni forces.

Cases 4 and 5

Cases 4 and 5 (Fig. 5) examine the effects when $\gamma_d < \gamma_p$. The end result is that radially outward surface flows are generated. Furthermore, a definitive toroidal flow (Δ in Fig. 6B) is also observed in the bulk fluid (Fig. 5B). The schematic representation of this flow pattern (Type II) is summarized in Fig. 6B where there are penetrating flow (A) due to the falling drop, rising flow (B) due to buoyancy, spreading flow (C) due to Marangoni effect, and toroidal flow (D) due to collision at the walls. Furthermore, the upward flow (B) is assisted by the spreading action (C′) during the early stages of contact when the droplet strikes the pool.

Of particular interest is Case 5 at ⅛-s exposure where $|\Delta\gamma|$ has been increased by 4.14 times and $|\Delta\rho|$ has been increased by 6.65 times with respect to Case 4. The spreading action (C′) due to Marangoni forces on initial droplet-pool contact is so overwhelming that the droplet does not penetrate into the pool but spreads out rapidly. Note the toroidal flows (Δ) near the walls as a result of this Marangoni effect (Case 5 — Fig. 6A). Case 5 indicates that the surface tension difference between the droplet and pool is critical in affecting both the droplet behavior and surface flow when the droplet first strikes the pool despite the larger increase in $|\Delta\gamma|$.

Case 6

A final test is performed in which Case 6 has the same $\Delta\rho$ as Case 5 but $|\Delta\gamma|$ is much less. At ⅛ s, the drop showed about the same penetration depth as Case 1 (Fig. 5A), but the initial spreading (C′) is not evident. Furthermore, at 1 s, no definitive flow pattern is noticeable and the flow is less intense than in Case 5. The drop appears to have risen to the top by buoyancy (shown schematically by flow B in Fig. 6B).

Discussion

Marangoni Interaction between Droplet and Pool

The water-alcohol physical model for GMAW indicates that Marangoni force not only controls the flow direction in the acrylic cell but also controls the intensity of the flow. It predominates over the buoyancy force due to density difference, the curvature force due surface curvature, and the stirring force due to the falling drop. This observation indicates that closer attention should be paid to the filler material and workpiece compatibility in terms of surface tension differences.

Inclusion Distribution

The larger questions that are being addressed in this study are the behavior and distribution of inclusions in the weld pool. The hollow glass beads in the liquid pool simulate the inclusions in the weld pool. Their behavior in the physical model may provide clues as to why inclusions segregate at certain regions of the weldment. Such an observation can be explained on the basis of the Marangoni interaction between the filler metal and the workpiece. If $\gamma_d > \gamma_p$, then the droplet will penetrate deep into the pool. As the time scale (time to freeze the pool) of the welding operation is of the order of 1 s, these inclusions may be frozen in when they reach the bottom of the pool within this time frame. If $\gamma_d < \gamma_p$, the droplet will spread out on the surface of the pool, and the inclusions may tend to segregate near the surface of the weldment.

Temperature-Induced Convection vs. Droplet-Induced Convection

Tsao and Wu (Ref. 21) reported a maximum calculated velocity of the order of 6–9 cm/s (2.4–3.5 in./s) for GMAW at 290 A solely on the basis of the $\partial\gamma/\partial T$ effect. The typical velocities measured in our physical model are of the order of 4–20 cm/s (1.6–7.9 in./s). It is reassuring to know that the droplet-induced Marangoni convection, through the Reynolds number, is of the same order of magnitude as the temperature-induced Marangoni convection, although it should be qualified that a closer examination of the surface tension similarity is needed to further substantiate the claim. This observation suggests that the role of the droplet-induced Marangoni flow should not be precluded from flow analyses in GMAW.

Physical Model Simplification

The physical model employed represents considerable simplification of the GMAW problem as described below.

Dilution of the Droplet

In the cases studied, some dilution of the droplet did occur. That is, the analyses did not address the part of the droplet that was submerged in Fig. 2B and C. It is necessary to account for this mixing by considering the convective and diffusive flows into the bulk liquid. Nevertheless, the physical model does indicate that despite the dilution effects, Marangoni flow is still very evident and dominant.

Frequency of Droplet Transfer

This physical model simulated the lower limit of the GMAW operation in terms of droplet mass transfer rates. Generally, the rate of spray transfer is a function of factors such as arc current, filler metal and shielding gas. For steel, it can vary from 0 to 80 drops per second for a 100- to 200-A arc in Ar (Ref. 9).

The effect of multiple droplets falling onto the pool in affecting weld pool flow circulation needs to be addressed. Naturally, if this scenario is modeled at room temperature, the flow that results will be quite difficult to characterize. In this instance, a mathematical model may be helpful in describing the flow patterns generated.

Weld Pool Convection

In welding, Marangoni flows will still be produced in the absence of filler metal, due to thermocapillary action. The direction of flow, and thus the weld pool shape, is established by the concentration of the surface active species (Refs. 5, 6).

The manner in which the weld pool convection can be altered by the filler metal with a different surface tension is dependent upon the magnitude between $\tau_{M(T)}$ (Equation 1) and $\tau_{M(C)}$ (Equation 2). Clearly, $\partial g/\partial T$ is small ($\sim 10^{-4}$ N/m-K) although $\partial T/\partial x$ is large due to the steep temperature gradients at the surface. It has been calculated that $\tau_{M(T)}$ is of the order of 100–200 Pa (Ref. 22). Incidentally, the gas shear over the free surface due to the shielding gas is of the order of 10–40 Pa (Ref. 23) and is not a significant shear to the weld pool surface. As for $\tau_{M(C)}$, it has been previously stated that $\partial \gamma/\partial x$ is large (probably a step function) when the drop hits the pool. Thus, $\tau_{M(C)}$ can be a considerable driving force at the initial stages of mixing. This effect should be borne in mind in mathematical modeling studies.

Concentration Dependency in the Weld Pool

It is well known that there is a relationship between γ and concentration (Ref. 16). It is reasonable to assume that there is a concentration dependency in the weld pool as a result of temperature variations via the solubilities. This dependency may lead to surface tension variations and thus create Marangoni flows. However, such event is unlikely since the weld pool is rigorously stirred and well mixed. The addition of filler metal to the weld pool represents a more drastic change in concentration than that caused by the weld pool temperature. Therefore, it is suspected that Marangoni flow due to concentration gradient as a result of solubility is not a major driving force in the weld pool.

Dynamic Similarity of the Physical Model

The physical model (acrylic cell) was designed on the basis of the dimensions typically found in weld pools. Furthermore, it also has the capability of simulating moving welding operations by means of moving the needle. No attempt was made to satisfy the dynamic similarity of Marangoni flows through the Marangoni number because the surface tension of the filler metal is usually unknown. Furthermore, the Marangoni number needs to be modified to account for the surface tension dependence on concentration. Efforts are being initiated to measure the surface tension of commercial filler metals by means of x-ray radiography on a sessile drop in this laboratory.

Conclusions

Using an isothermal water-alcohol physical model to simulate the filler metal (liquid droplet) and weld pool (bulk liquid) interaction of a gas metal arc welding operation, it was found that:

1. Marangoni flow due to the surface tension difference between the droplet and liquid pool is the dominant force that controls both the direction and intensity of the pool circulation.
2. If the droplet has a surface tension that is larger than the pool, then the droplet will penetrate deep into the liquid pool due to surface tension interaction between the droplet and the bulk liquid (Fig. 2B and Fig. 5A — Case 2).
3. If the droplet has a surface tension that is much smaller than the pool, then the droplet will spread out onto the surface as it impinges onto the pool (Fig. 2C and Fig. 5A — Case 5). In this instance, the momentum of the falling droplet was not sufficient to cause it to penetrate into the pool.

Acknowledgment

The authors wish to thank the Natural Sciences and Engineering Research Council of Canada for financial support of this investigation.

References

1. Heiple, C. R., and Roper, J. R. 1982. Mechanism for minor element effects on GTA fusion zone geometry. *Welding Journal* 61(10): 97-s to 102-s.
2. Walsh, D. W., and Savage, W. F. 1985. Autogenous GTA weldment — bead geometry variation due to minor elements. *Welding Journal* 64(2): 59-s to 62-s.
3. Oreper, G. M., Eagar, T. W., and Szekely, J. 1983. Convection in arc weld pools. *Welding Journal* 62(11): 307-s to 312-s.
4. Kou, S., and Wang, Y. H. 1985. Weld pool convection and its effects. *Welding Journal* 65 (9): 63-s to 70-s.
5. Zacharia, T., David, S. A., Vitek, J. M., and DebRoy, T. 1989. Weld pool development during GTA and laser welding of type 304 stainless steel, Part 1 — theoretical analysis. *Welding Journal* 68(12): 499-s to 509-s.
6. Zacharia, T., David, S. A., Vitek, J. M., and DebRoy, T. 1989. Weld pool development during GTA and laser welding of Type 304 stainless steel, Part 2 — experimental correlation. *Welding Journal* 68(12): 510-s to 519-s.
7. Lin, M. L., and Eagar, T. W. 1983. Influence of surface depression and convection on arc weld pool geometry. *Transport Phenomena in Materials Processing* ASME-PED 10, pp.63–69.
8. Savage, W. F. 1980. Solidification, segregation, and weld imperfections. Welding in the World 18, pp. 89–114.
9. *The Physics of Welding*. Second edition, 1986. J. F. Lancaster, ed., IIW, Pergamon Press, Oxford, Chapter 7.
10. Liu, S., and Siewert, T. A. 1989. Metal transfer in gas metal arc welding: droplet rate. *Welding Journal* 68(2): 52-s to 58-s.
11. Kim, Y. S. 1989. Metal transfer in gas metal arc welding. Ph.D. thesis, Department of Materials Science and Engineering, MIT, Cambridge, Mass.
12. Allemand, C. D., Schoeder, R., Ries, D., and Eagar, T. W. 1985. A method of filming metal transfer in welding. *Welding Journal* 64(1): 45–47.
13. Ueguri, S., Hara, K., and Komura, H. 1985. Study of metal transfer in pulsed GMA welding. *Welding Journal* 64(8): 242-s to 250-s.
14. Lu, M. J., and Kou, S. 1989. Power inputs in gas metal arc welding of aluminum —Part 1. *Welding Journal* 68(2): 382-s to 388-s.
15. Chen, J. H., Fan, D., He, Z. Q., Ye, J., and Luo, Y. C. 1989. A study of the mechanism for globular metal transfer from covered electrodes. *Welding Journal* 68(4): 145-s to 150-s.
16. Utigard, T. A., and Toguri, J. M. 1987. Surface segregation and surface tension of liquid mixtures. *Met. Trans.* B 18B, pp. 695–702.
17. Schwabe, D., and Scharmann, A. 1981. Marangoni convection in open boat and crucible. *J. Crystal Growth* 52, pp. 435–449.
18. *International Critical Tables of Numerical Data, Physics, Chemistry, and Technology*. Vol. 4, 1928. E.W. Washburn, ed., McGraw-Hill, New York, N.Y., pp. 465–467.
19. *International Critical Tables of Numerical Data, Physics. Chemistry, and Technology* Vol. 3, 1928. E.W. Washburn, ed., McGraw-Hill, New York, N.Y., pp. 116–117.
20. *International Critical Tables of Numerical Data, Physics. Chemistry. and Technology* Vol. 5, 1928. E.W. Washburn, ed., McGraw-Hill, New York, N. Y., pp. 15, 22.
21. Tsao, K. C., and Wu, C. S. 1988. Fluid flow and heat transfer in GMA weld pools. *Welding Journal* 67(3): 70-s to 75-s.
22. Choo, R. T. C. 1991. Mathematical modeling of heat and fluid flow phenomena in a mutually coupled welding arc and weld pool. Sc.D. thesis, Department of Materials Science and Engineering, MIT, Cambridge, Mass.
23. Choo, R. T. C., and Szekely, J. 1991. The effect of gas shear stress on Marangoni flows in arc welding. *Welding Journal* 70(9): 223-s to 233-s.